Control of Spurious Modes in a 9-Node Shell Element Based on the Assumed Strain Approach

Takahiro YAMADA*, Akira WADA**, and Fumio KIKUCHI*

* *College of Arts and Sciences, University of Tokyo, Tokyo*
** *Faculty of Engineering, Tokyo Institute of Technology, Tokyo*

A 9-node Lagrange shell element with uniform reduced integration (the 2×2 Gaussian quadrature) and a new spurious mode control procedure based on an assumed strain approach is presented. The strain fields are defined with interpolating the strains evaluated from the displacement field at certain sampling points. In the evaluation of element stiffness matrices, the 2×2 quadrature is employed for efficiency in the computational costs. However, some terms due to quadratic distributions of the assumed strain field cannot be evaluated by the 2×2 quadrature. Such terms lost by the use of the 2×2 quadrature are compensated by introducing additive matrices for the sake of stabilization. An extension to geometrically nonlinear problems is also presented.

Several numerical examples including both linear and geometrically nonlinear analyses of shells are presented, which demonstrate the good performance of the proposed element.

I. INTRODUCTION

In recent years, the degenerated shell approach is often employed to finite element procedure for plate and shell analysis. In this approach, a shell model is deduced from the three dimensional continuum theory by imposing appropriate kinematic assumptions. The 9-node Lagrange element based on this approach can express an arbitrary initial shape as biquadratic surface and deal with the interaction between membrane strains and bending strains inside an element. Thus the 9-node element seems to be efficient to general curved shell problems with geometrical nonlinearity.

However, elements of this type often exhibit well-known locking phenomena. Early attempts were made to avoid locking phenomena by the use of reduced/selective integration techniques (Parisch[1], Hughes and Liu[2] etc.). For problems with lightly constrained boundaries, these schemes cause rank deficiency and the elements include spurious singular modes. To avoid the locking phenomena without activating spurious singular modes, Belytschko and co-workers propose the reduced integration procedure with stabilization matrices[3),4)], which is an analogue of 'hourglass control' in 4-node element[5),6)]. Although the reduced integration procedure with the stabilization matrices is effective in computational costs, matrices based on such procedure include some numerical adjusting factors which have some ambiguity and lack physical backgrounds.

On the other hand, many researchers propose assumed strain approaches, in which strain field is defined with interpolating the strains evaluated from displacement field at certain sampling points (Bathe and Dvorkin[7], Huang and Hinton[8] and Park and Stanley[9] etc.). In these approaches, the 3×3 Gaussian quadrature rule is usually employed for numerical integration, and these approaches are less effective in computational costs than the uniformly reduced integration procedure with stabilization.

In this work, we propose a new stabilization procedure based on an assumed strain approach in 9-node shell element with uniform reduced integration (the 2×2 Gaussian quadrature) in order to obtain a shell element avoiding locking phenomena without spurious singular modes. In this procedure, the terms of the assumed strain field which cannot be evaluated with the 2×2 quadrature are calculated by separating and individually integrating such terms for the sake of stabilizing spurious modes. Thus our stabilization procedure does not include any numerical adjusting factors

in contrast to the stabilization procedure by Belytschko et al.[3),4)] The present formulation is effective in computational costs because of employing the 2×2 quadrature basically. Moreover we extend this procedure to geometrically nonlinear problems by the use of the Updated Lagrangian formulation.

To demonstrate the validity of the proposed approach, we analyze several shell problems including both linear and geometrically nonlinear ones. It is shown that our element neither exhibits any symptoms of membrane or shear locking nor spatial oscillations in the solutions.

II. ELEMENT DESCRIPTIONS

In this section, we summarize basic geometric and kinematic descriptions and definitions of a 9-node shell element. Our descriptions owe much to the work by Hughes and Liu[2)]. A modified representation of the lamina coordinate system originally given by Hughes and Liu[2)] is also presented.

2.1 Geometry and Kinematics

In this work, vector components of geometry and kinematics will be described in the global Cartesian coordinates. The initial configuration over a typical element Ω_e is described by the isoparametric mapping from cube with respect to $\xi, \eta, \zeta \in [-1, 1]$ to physical domain through

$$\mathbf{x}(\xi, \eta, \zeta) = \sum_{a=1}^{9} \{N_a(\xi, \eta)\mathbf{x}_a + \frac{1}{2} N_a(\xi, \eta) t_a \zeta \mathbf{X}_a\}, \tag{2.1}$$

where $\mathbf{x}$ denotes the position of the shell in the Cartesian coordinates; $\mathbf{x}_a$ is the position vector of nodal point a; $\mathbf{X}_a$ is a unit vector emanating from node a in the fiber direction which defines the normal direction at node a; t_a is the shell thickness at node a; N_a denotes the biquadratic Lagrange interpolation function; see Fig. 1. It is noted that each node of the element is located at the reference surface, which is taken as the middle surface of the shell.

By invoking the isoparametric hypothesis, the kinematics of the shell element can be expressed as

$$\mathbf{u}(\xi, \eta, \zeta) = \sum_{a=1}^{9} \{N_a(\xi, \eta)\mathbf{u}_a + \frac{1}{2} N_a(\xi, \eta) t_a \zeta \mathbf{U}_a\}, \tag{2.2}$$

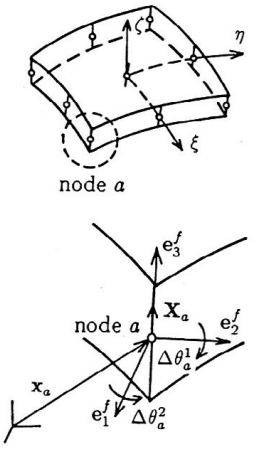

Fig. 1. 9-node shell element.

where $\mathbf{u}$ is the displacement field; $\mathbf{u}_a$ is the displacement at node a on the reference surface; $\mathbf{U}_a$ are the fiber displacement at node a.

Consequently, the deformed geometry is represented by the following expressions:

$$\mathbf{y} = \mathbf{x} + \mathbf{u}, \quad \mathbf{y}_a = \mathbf{x}_a + \mathbf{u}_a, \quad \mathbf{Y}_a = \mathbf{X}_a + \mathbf{U}_a. \tag{2.3}$$

where $\mathbf{y}$ is the deformed geometry; $\mathbf{y}_a$ is the position vector of nodal point a at deformed shape; $\mathbf{Y}_a$ is a unit vector emanating from node a in the fiber direction at deformed shape.

In nonlinear solution procedures, the vector $\mathbf{Y}_a$ is required to remain a unit vector so that nodal fibers are inextensible. In practice, a trial value of $\mathbf{U}_a$ is calculated and projected radially to maintain the inextensibility; see Hughes and Liu[2)] for details.

2.2 Lamina Coordinate System

We introduce a local Cartesian coordinate system called the 'lamina' coordinate system to measure strains and stresses. The lamina coordinate system should be chosen so that the strain and stress fields measured in this coordinate system will be able to represent the constant states in each element to pass the patch test.

To define the lamina coordinate system, we first introduce a Cartesian coordinate system called the 'center' coordinate system which is located at the center ($\xi = \eta = \zeta = 0$) in the individual elements. The basis vectors $\mathbf{e}_i^c$ of the center coordinate system is chosen so that the angle formed by $\mathbf{e}_1^c$ and ξ directions is equal to that formed by $\mathbf{e}_2^c$ and η directions in the current configuration; see Fig. 2. The $\mathbf{e}_3^c$ direction is the normal direction to the element surface.

Associated with the above center coordinate system, the basis vectors $\mathbf{e}_i^l$ of the lamina coordinate system at each sampling point are determined in the current configuration as follows:

$$\mathbf{e}_3^l = \mathbf{y}_{,\xi} \times \mathbf{y}_{,\eta} / |\mathbf{y}_{,\xi} \times \mathbf{y}_{,\eta}|, \quad \mathbf{e}_2^l = \mathbf{e}_3^l \times \mathbf{e}_1^c / |\mathbf{e}_3^l \times \mathbf{e}_1^c|, \quad \mathbf{e}_1^l = \mathbf{e}_2^l \times \mathbf{e}_3^l, \tag{2.4}$$

where the comma denotes partial differential (i.e. $\mathbf{y}_{,\xi} = \partial \mathbf{y}/\partial \xi$) and '$\times$' denotes the vector product. For the purpose of involving the plane stress hypothesis, we employ $\mathbf{e}_1^l$ and $\mathbf{e}_2^l$ directions which are tangent to the element lamina, and $\mathbf{e}_3^l$ direction which is normal to the element lamina. The lamina basis rotates rigidly as the element deforms. It is noted that the lamina coordinate systems at all sampling points over an element coincide in the direction when nine nodes are on a common plane. Thus, strain and stress fields measured in the lamina coordinates can represent the constant states independently of the form of interpolation when the element is flat.

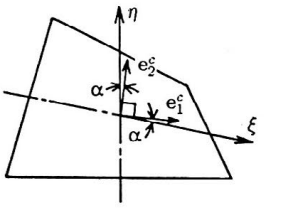

Fig. 2. Center coordinate system.

Consequently, the matrix which transform quantities from the global coordinate system to the lamina coordinate system is obtained by

$$\mathbf{q} = [\mathbf{e}_1^l \; \mathbf{e}_2^l \; \mathbf{e}_3^l]^t. \tag{2.5}$$

Clearly, $\mathbf{q}$ is orthonormal.

2.3 Fiber Coordinate System

In the proposed element, five degrees of freedom are employed at each node. At each node, a local Cartesian coordinate system called the 'fiber' coordinate system is defined and used as the reference frame for the incremental fiber displacement $\Delta \mathbf{U}_a$. The orthonormal basis vectors of the fiber coordinate system are $\mathbf{e}_i^f$ (The nodal subscript 'a' is omitted here for clarity.). We employ the algorithm presented by Liu, Law, Lam and Belytschko[4] to specify the directions of $\mathbf{e}_i^f$. The direction of $\mathbf{e}_3^f$ is always equal to that of the current fiber vector $\mathbf{Y}_a$, and the other two basis vectors $\mathbf{e}_1^f$ and $\mathbf{e}_2^f$ are uniquely defined as orthonormal bases.

Here we introduce the generalized incremental displacement vector $\Delta \mathbf{d}_a$ with five components (three translations and two rotations) at nodal point a as

$$\Delta \mathbf{d}_a = \lfloor \Delta u_a^1 \; \Delta u_a^2 \; \Delta u_a^3 \; \Delta \theta_a^1 \; \Delta \theta_a^2 \rfloor^t, \tag{2.6}$$

where the superscript 't' denotes the transpose. $\Delta \theta_a^1$ and $\Delta \theta_a^2$ are incremental rotations about the basis vectors $\mathbf{e}_1^f$ and $\mathbf{e}_2^f$ respectively. Invoking inextensibility of the nodal fibers, the linearized relationship between the components of the incremental fiber displacement $\Delta \mathbf{U}_a$ and the incremental rotations is given by using the fiber coordinate system as

$$\begin{Bmatrix} \Delta \mathbf{u}_a \\ \Delta \mathbf{U}_a \end{Bmatrix} = \mathbf{R}_a \Delta \mathbf{d}_a, \tag{2.7}$$

where $\mathbf{R}_a$ is 6×5 matrix defined by

$$\mathbf{R}_a = \begin{bmatrix} \mathbf{I}_3 & \mathbf{0}_{3\times 2} \\ \mathbf{0}_{3\times 3} & \mathbf{r}_a \end{bmatrix}, \quad \mathbf{r}_a = \left[\mathbf{e}_1^f \; \mathbf{e}_2^f \right], \tag{2.8}$$

with $\mathbf{I}_n$ being the $n \times n$ unit matrix and $\mathbf{0}_{n\times m}$ being the $n \times m$ zero matrix.

Remarks. In the linear formulation, the current configuration is equal to (or indistinguishable from) the initial configuration. Thus, all the local coordinate systems (center, lamina and fiber coordinate systems) are calculated in the initial configuration.

III. FINITE ELEMENT FORMULATION

In this section, a finite element formulation based on an assumed strain approach is presented. Here, the formulation is restricted to linear elastic problems for simplicity. Thus, we need not use incremental displacement, and hence we omit the symbol Δ of increment in the descriptions below.

3.1 Assumed Strain Field

In this work, the strain field is assumed independently on each layer (ζ =const. surface). In the following discussion we consider the strain field on a certain layer and omit the indication of the ζ coordinate for clarity, but the strain field is actually dependent on ζ as well.

The components of the assumed strain field ϵ are measured in the lamina coordinate system and consist of in-plane strains ϵ_{11}, ϵ_{22}, ϵ_{12} and transverse shear strains ϵ_{31}, ϵ_{23}, totaling to five components, except the axial strain ϵ_{33} in the normal direction. The strain component ϵ_{33} is calculated, if necessary, from the other strain components by the use of the plane stress hypothesis. To avoid locking phenomena, the assumed strain field should be expressed as polynomials of a lower degree than those of the strain derived from the displacement field. Further, the assumed strain field should also be able to represent all the displacement modes except for rigid body modes in order to cause no spurious mode.

Considering the above conditions, we choose the sampling points which are located at four 2×2 Gaussian quadrature points ($\pm 1/\sqrt{3}$, $\pm 1/\sqrt{3}$) plus four points (0 , $\pm 1/\sqrt{3}$) and ($\pm 1/\sqrt{3}$, 0), totaling to eight points; see Fig. 3. Strains evaluated from the displacement field at each sampling point are obtained by

$$\gamma_{ij}^{[p,q]} = \frac{1}{2}\left(\frac{\partial u_i^l}{\partial x_j^l} + \frac{\partial u_j^l}{\partial x_i^l}\right), \tag{3.1}$$

where superscript 'l' denotes appropriate quantity measured in the lamina coordinates and superscript '$[p,q]$' denotes appropriate quantity evaluated at a sampling point $[p,q]$. The left hand side in equation (3.1) is the value evaluated at the sampling point $[p,q]$.

Interpolating these strains, we employ the assumed strain field as

$$\epsilon_{11} = \sum_{p=1}^{2}\sum_{q=1}^{3} L_p(\xi)H_q(\eta)\gamma_{11}^{[p,q]}, \quad \epsilon_{22} = \sum_{p=1}^{3}\sum_{q=1}^{2} H_p(\xi)L_q(\eta)\gamma_{22}^{[p,q]},$$

$$\epsilon_{31} = \sum_{p=1}^{2}\sum_{q=1}^{3} L_p(\xi)H_q(\eta)\gamma_{31}^{[p,q]}, \quad \epsilon_{23} = \sum_{p=1}^{3}\sum_{q=1}^{2} H_p(\xi)L_q(\eta)\gamma_{23}^{[p,q]}, \quad \epsilon_{12} = \sum_{p=1}^{2}\sum_{q=1}^{2} L_p(\xi)L_q(\eta)\gamma_{12}^{[p,q]}. \tag{3.2}$$

where $L_i(s)$ and $H_i(s)$ are interpolate functions given by

$$L_1(s) = \frac{1}{2}(1 - \sqrt{3}s), \quad L_2(s) = \frac{1}{2}(1 + \sqrt{3}s), \tag{3.3}$$

$$H_1(s) = -\frac{\sqrt{3}}{2}s(1 - \sqrt{3}s), \quad H_2(s) = \frac{\sqrt{3}}{2}s(1 + \sqrt{3}s), \quad H_3(s) = (1 - \sqrt{3}s)(1 + \sqrt{3}s). \tag{3.4}$$

It is noted that ϵ_{11}, ϵ_{31} are linear in ξ and quadratic in η, ϵ_{22}, ϵ_{23} are linear in η and quadratic in ξ and ϵ_{12} is linear in both ξ and η. This strain field is chosen so that it will avoid locking phenomena and cause no spurious singular mode.

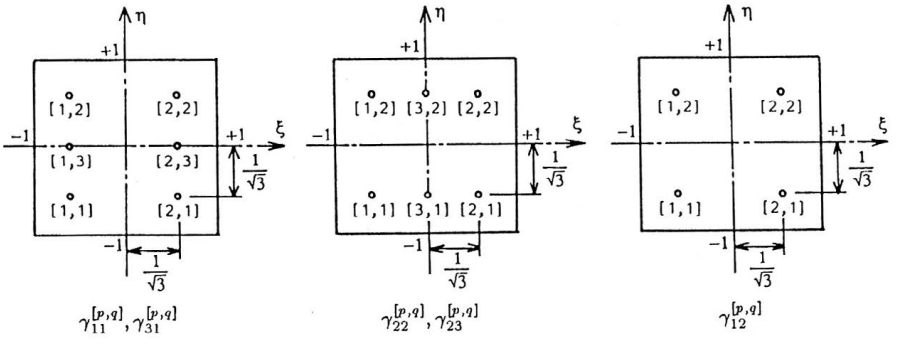

Fig. 3. Sampling points $[p,q]$ for strains.

This strain field will be expressed as a form with the quadratic terms added to the bilinear terms:

$$\begin{aligned}
\epsilon_{11} &= \sum_{p=1}^{2}\sum_{q=1}^{2} L_p(\xi)L_q(\eta)\gamma_{11}^{[p,q]} + (1-3\eta^2)\sum_{p=1}^{2} L_p(\xi)\bar{\gamma}_{11}^{[p]},\\
\epsilon_{31} &= \sum_{p=1}^{2}\sum_{q=1}^{2} L_p(\xi)L_q(\eta)\gamma_{31}^{[p,q]} + (1-3\eta^2)\sum_{p=1}^{2} L_p(\xi)\bar{\gamma}_{31}^{[p]},\\
\epsilon_{22} &= \sum_{p=1}^{2}\sum_{q=1}^{2} L_p(\xi)L_q(\eta)\gamma_{22}^{[p,q]} + (1-3\xi^2)\sum_{q=1}^{2} L_q(\eta)\bar{\gamma}_{22}^{[q]},\\
\epsilon_{23} &= \sum_{p=1}^{2}\sum_{q=1}^{2} L_p(\xi)L_q(\eta)\gamma_{23}^{[p,q]} + (1-3\xi^2)\sum_{q=1}^{2} L_q(\eta)\bar{\gamma}_{23}^{[q]},
\end{aligned} \tag{3.5}$$

where

$$\begin{aligned}
&\bar{\gamma}_{11}^{[p]} = \gamma_{11}^{[p,3]} - (\gamma_{11}^{[p,1]} + \gamma_{11}^{[p,2]})/2, \quad \bar{\gamma}_{31}^{[p]} = \gamma_{31}^{[p,3]} - (\gamma_{31}^{[p,1]} + \gamma_{31}^{[p,2]})/2,\\
&\bar{\gamma}_{22}^{[q]} = \gamma_{22}^{[3,q]} - (\gamma_{22}^{[1,q]} + \gamma_{22}^{[2,q]})/2, \quad \bar{\gamma}_{23}^{[q]} = \gamma_{23}^{[3,q]} - (\gamma_{23}^{[1,q]} + \gamma_{23}^{[2,q]})/2.
\end{aligned} \tag{3.6}$$

According to the above strain field, the matrix $\bar{\mathbf{B}}_a$, which transforms the nodal displacement vector in the global coordinates into the assumed strain field is defined as

$$\lfloor \epsilon_{11}\ \epsilon_{22}\ 2\epsilon_{12}\ 2\epsilon_{23}\ 2\epsilon_{31} \rfloor^t = \sum_{a=1}^{9} \bar{\mathbf{B}}_a(\xi,\eta,\zeta)\mathbf{R}_a\mathbf{d}_a. \tag{3.7}$$

Considering the matrix $\bar{\mathbf{B}}_a$, we introduce the following matrices:

$$\mathbf{B}_a^{[p,q]} = \begin{bmatrix} B_1^{[p,q]} & 0 & 0 & B_4^{[p,q]} & 0 & 0\\ 0 & B_2^{[p,q]} & 0 & 0 & B_5^{[p,q]} & 0\\ B_2^{[p,q]} & B_1^{[p,q]} & 0 & B_5^{[p,q]} & B_4^{[p,q]} & 0\\ 0 & B_3^{[p,q]} & B_2^{[p,q]} & 0 & B_6^{[p,q]} & B_5^{[p,q]}\\ B_3^{[p,q]} & 0 & B_1^{[p,q]} & B_6^{[p,q]} & 0 & B_4^{[p,q]} \end{bmatrix} \mathbf{Q}^{[p,q]}, \tag{3.8}$$

$$\begin{aligned}
\tilde{\mathbf{B}}_a^{\xi[p]} = {} & \begin{bmatrix} B_1^{[p,3]} & 0 & 0 & B_4^{[p,3]} & 0 & 0\\ 0 & 0 & 0 & 0 & 0 & 0\\ 0 & 0 & 0 & 0 & 0 & 0\\ 0 & 0 & 0 & 0 & 0 & 0\\ B_3^{[p,3]} & 0 & B_1^{[p,3]} & B_6^{[p,3]} & 0 & B_4^{[p,3]} \end{bmatrix} \mathbf{Q}^{[p,3]}\\
& -\frac{1}{2}\begin{bmatrix} B_1^{[p,1]} & 0 & 0 & B_4^{[p,1]} & 0 & 0\\ 0 & 0 & 0 & 0 & 0 & 0\\ 0 & 0 & 0 & 0 & 0 & 0\\ 0 & 0 & 0 & 0 & 0 & 0\\ B_3^{[p,1]} & 0 & B_1^{[p,1]} & B_6^{[p,1]} & 0 & B_4^{[p,1]} \end{bmatrix} \mathbf{Q}^{[p,1]} - \frac{1}{2}\begin{bmatrix} B_1^{[p,2]} & 0 & 0 & B_4^{[p,2]} & 0 & 0\\ 0 & 0 & 0 & 0 & 0 & 0\\ 0 & 0 & 0 & 0 & 0 & 0\\ 0 & 0 & 0 & 0 & 0 & 0\\ B_3^{[p,2]} & 0 & B_1^{[p,2]} & B_6^{[p,2]} & 0 & B_4^{[p,2]} \end{bmatrix} \mathbf{Q}^{[p,2]},
\end{aligned} \tag{3.9}$$

$$\begin{aligned}
\tilde{\mathbf{B}}_a^{\eta[q]} = {} & \begin{bmatrix} 0 & 0 & 0 & 0 & 0 & 0\\ 0 & B_2^{[3,q]} & 0 & 0 & B_5^{[3,q]} & 0\\ 0 & 0 & 0 & 0 & 0 & 0\\ 0 & B_3^{[3,q]} & B_2^{[3,q]} & 0 & B_6^{[3,q]} & B_5^{[3,q]}\\ 0 & 0 & 0 & 0 & 0 & 0 \end{bmatrix} \mathbf{Q}^{[3,q]}\\
& -\frac{1}{2}\begin{bmatrix} 0 & 0 & 0 & 0 & 0 & 0\\ 0 & B_2^{[1,q]} & 0 & 0 & B_5^{[1,q]} & 0\\ 0 & 0 & 0 & 0 & 0 & 0\\ 0 & B_3^{[1,q]} & B_2^{[1,q]} & 0 & B_6^{[1,q]} & B_5^{[1,q]}\\ 0 & 0 & 0 & 0 & 0 & 0 \end{bmatrix} \mathbf{Q}^{[1,q]} - \frac{1}{2}\begin{bmatrix} 0 & 0 & 0 & 0 & 0 & 0\\ 0 & B_2^{[2,q]} & 0 & 0 & B_5^{[2,q]} & 0\\ 0 & 0 & 0 & 0 & 0 & 0\\ 0 & B_3^{[2,q]} & B_2^{[2,q]} & 0 & B_6^{[2,q]} & B_5^{[2,q]}\\ 0 & 0 & 0 & 0 & 0 & 0 \end{bmatrix} \mathbf{Q}^{[2,q]},
\end{aligned} \tag{3.10}$$

where

$$B_k^{[p,q]} = \begin{cases} \partial N_a/\partial x_k^l & k = 1,2,3\ , \\ \partial \tilde{N}_a/\partial x_{k-3}^l & k = 4,5,6\ , \end{cases} \quad \text{at sampling point } [p,q] \tag{3.11}$$

and $\tilde{N}_a$ is the modified shape function for the fiber part given by

$$\tilde{N}_a = \frac{1}{2} N_a(\xi,\eta) t_a \zeta \quad (\text{ no sum on } a\ ). \tag{3.12}$$

$\mathbf{Q}^{[p,q]}$ is the matrix which transforms the displacement vector from the global coordinates to the lamina coordinates at the sampling point $[p,q]$ as follows:

$$\begin{Bmatrix} \mathbf{u}_a^l \\ \mathbf{U}_a^l \end{Bmatrix} = \mathbf{Q}^{[p,q]} \begin{Bmatrix} \mathbf{u}_a \\ \mathbf{U}_a \end{Bmatrix}, \quad \mathbf{Q}^{[p,q]} = \begin{bmatrix} \mathbf{q}^{[p,q]} & \mathbf{0}_{3\times 3} \\ \mathbf{0}_{3\times 3} & \mathbf{q}^{[p,q]} \end{bmatrix}. \tag{3.13}$$

Here $\mathbf{q}^{[p,q]}$ denotes $\mathbf{q}$ in equation (2.5) at sampling point $[p,q]$. The matrices $\mathbf{B}_a^{[p,q]}$, $\tilde{\mathbf{B}}_a^{\xi[p]}$ and $\tilde{\mathbf{B}}_a^{\eta[q]}$ give the strains through

$$\lfloor \gamma_{11}^{[p,q]}\ \gamma_{22}^{[p,q]}\ 2\gamma_{12}^{[p,q]}\ 2\gamma_{23}^{[p,q]}\ 2\gamma_{31}^{[p,q]} \rfloor^t = \sum_{a=1}^{9} \mathbf{B}_a^{[p,q]} \mathbf{R}_a \mathbf{d}_a, \tag{3.14}$$

$$\lfloor \bar{\gamma}_{11}^{[p]}\ 0\ 0\ 0\ 2\bar{\gamma}_{31}^{[p]} \rfloor^t = \sum_{a=1}^{9} \tilde{\mathbf{B}}_a^{\xi[p]} \mathbf{R}_a \mathbf{d}_a, \quad \lfloor 0\ \bar{\gamma}_{22}^{[q]}\ 0\ 2\bar{\gamma}_{23}^{[q]}\ 0 \rfloor^t = \sum_{a=1}^{9} \tilde{\mathbf{B}}_a^{\eta[q]} \mathbf{R}_a \mathbf{d}_a. \tag{3.15}$$

Thus, the matrix $\bar{\mathbf{B}}_a$ can be shown to be

$$\bar{\mathbf{B}}_a(\xi,\eta,\zeta) = \sum_{p=1}^{2}\sum_{q=1}^{2} L_p(\xi) L_q(\eta) \mathbf{B}_a^{[p,q]} + (1-3\eta^2) \sum_{p=1}^{2} L_p(\xi) \tilde{\mathbf{B}}_a^{\xi[p]} + (1-3\xi^2) \sum_{q=1}^{2} L_q(\eta) \tilde{\mathbf{B}}_a^{\eta[q]}. \tag{3.16}$$

Remarks. Since the strain distributions derived from the displacement field are linear with respect to ζ in the case of flat plates, the assumed strain field is also at most linear in ζ. Considering the strain distribution derived from the displacement field, in-plane components of the assumed strain field ϵ_{11}, ϵ_{22}, ϵ_{12} are linear across the thickness and transverse shear components ϵ_{23}, ϵ_{31} are constant.

3.2 Evaluation of Stiffness Matrix

By the use of the above assumed strain field, an element stiffness matrix is given by

$$\mathbf{k}_{ab} = \int_{-1}^{1}\int_{-1}^{1}\int_{-1}^{1} \bar{\mathbf{B}}_a \mathbf{D} \bar{\mathbf{B}}_b J d\xi d\eta d\zeta, \tag{3.17}$$

where J denotes Jacobian and $\mathbf{D}$ denotes the material response matrix. We can decompose the stiffness matrix into two parts: a part $\mathbf{k}^{\mathrm{R}}$ derived from only bilinear distribution of the assumed strain field and another remaining part $\mathbf{k}^{\mathrm{S}}$ as

$$\mathbf{k}_{ab} = \mathbf{k}_{ab}^{\mathrm{R}} + \mathbf{k}_{ab}^{\mathrm{S}}. \tag{3.18}$$

Thus $\mathbf{k}_{ab}^{\mathrm{R}}$ can be expressed as

$$\mathbf{k}_{ab}^{\mathrm{R}} = \sum_{p=1}^{2}\sum_{q=1}^{2} \int_{-1}^{1}\int_{-1}^{1}\int_{-1}^{1} L_p(\xi) L_q(\eta) \mathbf{B}_a^{[p,q]} \mathbf{D} \mathbf{B}_b^{[p,q]} J d\xi d\eta d\zeta. \tag{3.19}$$

Note that $\mathbf{k}_{ab}^{\mathrm{R}}$ can be evaluated almost exactly by the 2×2 Gaussian quadrature, which is a numerical integration scheme with accuracy up to third order polynomials. Thus employing th 2×2 quadrature in $\mathbf{k}_{ab}^{\mathrm{R}}$, its summation form is obtained by

$$\mathbf{k}_{ab}^{\mathrm{R}} = \sum_{p=1}^{2}\sum_{q=1}^{2} \int_{-1}^{1} \mathbf{B}_a^{[p,q]} \mathbf{D} \mathbf{B}_b^{[p,q]} J^{[p,q]} d\zeta. \tag{3.20}$$

It is noted that the value of quadrature weight is equal to 1. This is nothing but the stiffness matrix obtained by an ordinary reduced integration.

With respect to another part of the stiffness matrix, we introduce some approximate relationships. Assuming that the element is low distorted (i.e. J is constant over an element) and the material response matrix $\mathbf{D}$ is constant over an element, the following approximate relationship can be obtained:

$$\int_{-1}^{1}(1-3s^2)\mathbf{D}Jds=0,\quad \int_{-1}^{1}(1-3s^2)s\mathbf{D}Jds=0,\quad \int_{-1}^{1}(1-3s^2)^2\mathbf{D}Jds=\frac{8}{5}\mathbf{D}J. \tag{3.21}$$

By applying these equations, the matrix $\mathbf{k}_{ab}^{S}$ can be shown to be

$$\mathbf{k}_{ab}^{S}=\sum_{p=1}^{2}\frac{8}{5}\int_{-1}^{1}\tilde{\mathbf{B}}_a^{\xi[p]}\mathbf{D}\tilde{\mathbf{B}}_b^{\xi[p]}J^{[p,3]}d\zeta+\sum_{q=1}^{2}\frac{8}{5}\int_{-1}^{1}\tilde{\mathbf{B}}_a^{\eta[q]}\mathbf{D}\tilde{\mathbf{B}}_b^{\eta[q]}J^{[3,q]}d\zeta \tag{3.22}$$

It is noted that J will be the value at each sampling point in equation (3.21) in order to evaluate the numerical integration as exactly as possible. The matrix $\mathbf{k}_{ab}^{S}$ is obtained by integrating only quadratic distribution terms of the assumed strain field, and corresponds to stabilization matrix resisting the spurious spurious modes.

The matrix $\mathbf{k}_{ab}^{S}$ is also an analogue of the stabilization matrix proposed by Belytschko et al.[3),4)] The stabilization scheme by Belytschko et al. is based on the use of an artificial displacement vector including spurious modes. Therefore, it needs artificial scaling to assure physically reasonable behaviors for the numerical solutions obtained by its use. In our formulation, the stabilization matrix is derived from quadratic distribution terms of the assumed strain field. Thus it has clear physical backgrounds in contrast to the one by Belytschko et al.

It is noted that for numerical integration in ζ direction as shown in equations (3.20) and (3.22), we employ the 3 point Simpson rule.

IV. NONLINEAR FORMULATION

In this section, we propose an extension of our formulation to geometrically nonlinear problems. In this work, we employ the Updated Lagrangian formulation to deal with geometrical nonlinearity. In the Updated Lagrangian formulation, all the current variables are referred to the current configuration for each new load increment (say at step n). In our nonlinear formulation, the interpolation concept of strains in section 3.1 is applied to the incremental strains given by

$$\Delta\gamma_{ij}^{[p,q]}=\frac{1}{2}\left(\frac{\partial\Delta u_i^l}{\partial y_j^l}+\frac{\partial\Delta u_j^l}{\partial y_i^l}\right), \tag{4.1}$$

where y_i is the deformed geometry as shown in equation (2.3). Moreover, with respect to the matrix $\tilde{\mathbf{B}}_a$, the derivatives in the initial configuration are substituted into those in the current configuration.

Similar to the strain field, we assume that the Cauchy stress field τ_{ij} is expressed as

$$\begin{aligned}
\tau_{11}&=\sum_{p=1}^{2}\sum_{q=1}^{2}L_p(\xi)L_q(\eta)\sigma_{11}^{[p,q]}+(1-\eta^2)\sum_{p=1}^{2}L_p(\xi)\bar{\sigma}_{11}^{[p]},\\
\tau_{31}&=\sum_{p=1}^{2}\sum_{p=1}^{2}L_p(\xi)L_q(\eta)\sigma_{31}^{[p,q]}+(1-\eta^2)\sum_{p=1}^{2}L_p(\xi)\bar{\sigma}_{31}^{[p]},\\
\tau_{22}&=\sum_{p=1}^{2}\sum_{q=1}^{2}L_p(\xi)L_q(\eta)\sigma_{22}^{[p,q]}+(1-\xi^2)\sum_{q=1}^{2}L_q(\eta)\bar{\sigma}_{22}^{[q]},\\
\tau_{23}&=\sum_{p=1}^{2}\sum_{q=1}^{2}L_p(\xi)L_q(\eta)\sigma_{23}^{[p,q]}+(1-\xi^2)\sum_{q=1}^{2}L_q(\eta)\bar{\sigma}_{23}^{[q]},\\
\tau_{12}&=\sum_{p=1}^{2}\sum_{q=1}^{2}L_p(\xi)L_q(\eta)\sigma_{12}^{[p,q]},
\end{aligned} \tag{4.1}$$

where $\sigma_{ij}^{[p,q]}$ is the Cauchy stress at sampling point $[p,q]$ and $\bar{\sigma}_{ij}^{[p]}$ is the term of the second distribution resisting spurious singular modes. $\bar{\sigma}_{ij}^{[p]}$ corresponds to the strain components $\bar{\gamma}_{ij}^{[p]}$.

Here, we introduce the following approximate relation to evaluate $\bar{\sigma}_{ij}^{[p]}$. We assume that $\bar{\sigma}_{ij}^{[p]}$ will be derived from only $\bar{\gamma}_{ij}^{[p]}$ through

$$\sigma_{ij}^{[p](n+1)} = \bar{\sigma}_{ij}^{[p](n)} + c_{ijij}\Delta\bar{\gamma}_{ij}^{[p]}, \quad (\text{ no sum on } i, j\ ) \tag{4.2}$$

where superscript '(n)' denotes the quantities at step n and $\Delta\bar{\gamma}_{ij}^{[p]}$ is incremental strain of $\bar{\gamma}_{ij}^{[p]}$. c_{ijkl} is a material response tensor.

On the other hand, the Cauchy stress components $\sigma_{ij}^{[p,q]}$ at the 2×2 quadrature points are evaluated from $\Delta\gamma_{ij}^{[p,q]}$. In calculating them practically, we employ the co-rotational approximation proposed by Hughes et al.[3),10)]

With respect to the internal force vector, the same assumptions as those in the evaluation of the stiffness matrix are employed. Similarly to equations (3.20) and (3.22), the internal force vector can be shown to be

$$\mathbf{f}_a^{\text{int}} = \sum_{p=1}^{2}\sum_{q=1}^{2}\int_{-1}^{1}(\mathbf{B}_a^{[p,q]})^t\sigma_{\text{vec}}^{[p,q]}J^{[p,q]}d\zeta + \sum_{p=1}^{2}\frac{8}{5}\int_{-1}^{1}(\tilde{\mathbf{B}}_a^{\xi[p]})^t\bar{\sigma}_{\text{vec}}^{\xi[p]}J^{[p,3]}d\zeta + \sum_{q=1}^{2}\frac{8}{5}\int_{-1}^{1}(\tilde{\mathbf{B}}_a^{\eta[q]})^t\bar{\sigma}_{\text{vec}}^{\eta[q]}J^{[3,q]}d\zeta, \tag{4.3}$$

where

$$\sigma_{\text{vec}}^{[p,q]} = \lfloor\sigma_{11}^{[p,q]}\ \sigma_{22}^{[p,q]}\ \sigma_{12}^{[p,q]}\ \sigma_{23}^{[p,q]}\ \sigma_{31}^{[p,q]}\rfloor^t, \tag{4.4}$$

$$\bar{\sigma}_{\text{vec}}^{\xi[p]} = \lfloor\bar{\sigma}_{11}^{[p]}\,0\,0\,0\,\bar{\sigma}_{31}^{[p]}\rfloor^t, \quad \bar{\sigma}_{\text{vec}}^{\eta[q]} = \lfloor 0\,\bar{\sigma}_{22}^{[q]}\,0\,\bar{\sigma}_{23}^{[q]}\,0\rfloor^t. \tag{4.5}$$

Further, geometrical stiffness matrices are evaluated by the 2×2 quadrature since the second distributions of the stresses merely reflect to geometrical nonlinearity over an element.

Remarks. It is also possible in linear formulation to assume the same form of the stress field as (4.2). In fact, the final results derived from the assumed stress field in (4.2) coincide with the former results derived from the assumptions in (3.20). However the former formulation in section 3.2 is more easily implemented than the latter.

V. NUMERICAL EXAMPLES

In this section, several numerical examples are given to see the efficiency of this approach. Some of the problems included here have been recently suggested as a set of benchmarks for testing the numerical behavior of shell elements (MacNeal and Harder[11)]).

5.1 Eigenanalysis of Stiffness Matrix

Eigenanalysis of the stiffness matrix of a single element is performed for various shapes. It is found that for this element there are only six zero eigenvalues, all of which are associated with rigid modes. This fact means that this element includes no spurious singular mode.

5.2 Patch Tests

Patch tests are performed on shells for meshes of arbitrary quadrilaterals of type shown in fig.4. The results indicate that out element can represent the fields of constant moment, constant twist or transverse shear forces and constant in-plane forces when the elements are flat. Thus, our element passes patch tests and its convergence is assured.

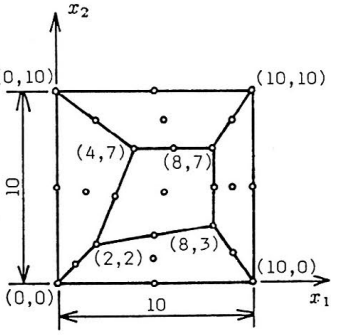

t = 0.01
E = 2.1 × 10^6
ν = 0.3

Fig. 4. Employed patch of elements.

5.3 A Pinched Cylinder with Diaphragms

The pinched cylinder shown in Fig. 5 is frequently used as a severe test for inextensional bending modes; it exhibits almost no membrane strains. Because of symmetry, only one eighth of the shell is modeled with uniform meshes as shown in the figure (5×5 nodes in the figure).

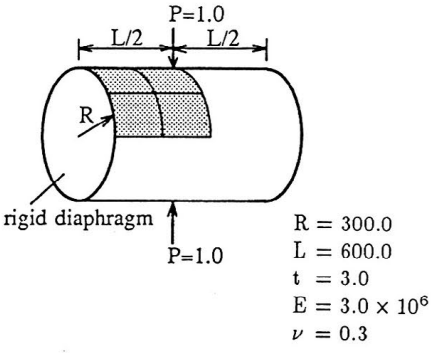

Fig. 5. A pinched cylinder with end diaphragms.

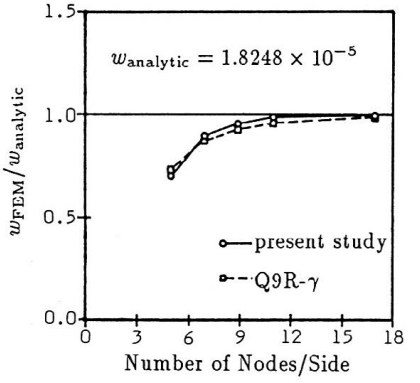

Fig. 6. Displacement convergence study for a pinched cylinder.

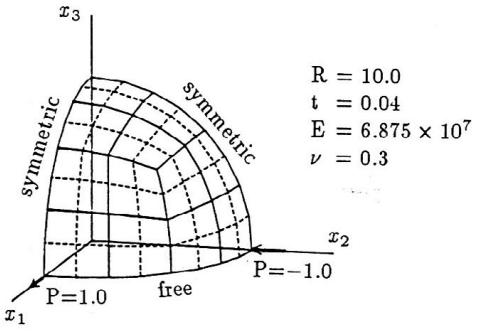

Fig. 7. A hemispherical shell.

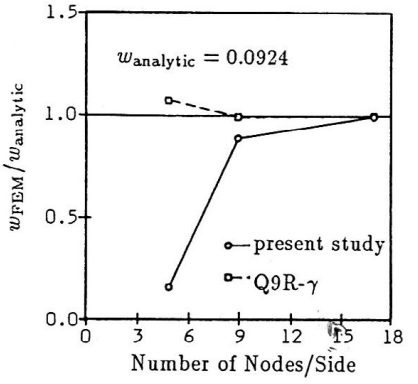

Fig. 8. Displacement convergence study for a hemispherical shell.

The results for normalized radial displacement at the loading point are presented in Fig. 6. Analytical results are taken from Belytschko et al[4]. A comparison is provided with the performance of Q9R-γ, the 9-node Lagrangian element with uniformly reduced integration involving γ-stabilization proposed by Belytschko et al[4]. It is shown that this element appears to perform slightly better in comparison with Q9R-γ.

5.4 A Hemispherical Shell

The hemispherical shell problem shown in Fig. 7 is another challenging test problem of element ability to represent inextensional modes, it exhibits almost no membrane strains. It is also useful for checking the ability to handle rigid body rotations about normals to the shell surface, since most sections of the shell rotate almost as rigid bodies under given loads. Due to symmetry, one quarter of the shell is modeled by 5, 9 and 17 nodes per each side as shown in Fig. 7. A comparison is again provided with the performance of Q9R-γ.

The convergence curves for normalized displacement at the loading point are depicted in Fig. 8. These results indicate that element Q9R-γ is better than the present element for coarse meshes. The local Cartesian coordinate system, in which the assumed strain fields are measured in our approach, is unsuitable for shell problems with highly curved geometry like this. Thus, accuracy intends to fall in coarse meshes. However, the results appear to be acceptable for finer meshes.

5.5 A Cantilever in Large Deflection

A cantilever subjected to a bending moment at the free end is analyzed by using the single

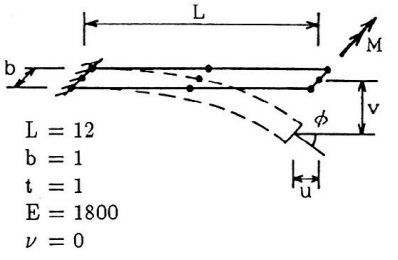

Fig. 9. An elastic cantilever beam.

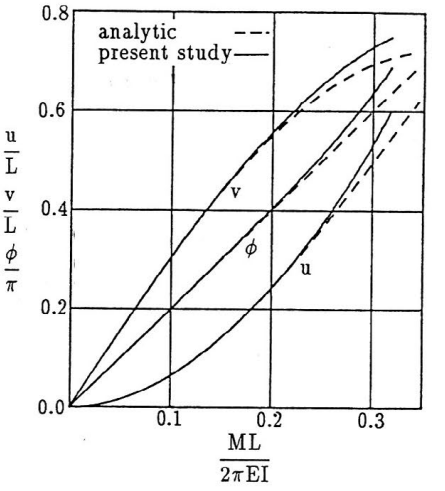

Fig. 10. Load displacement curve for a cantilever.

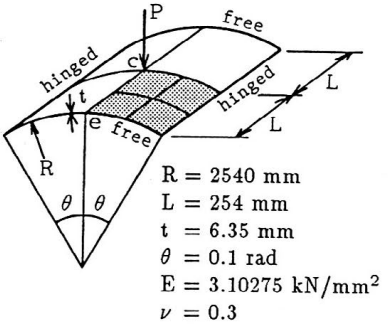

Fig. 11. A hinged cylindrical shell under concentrated load.

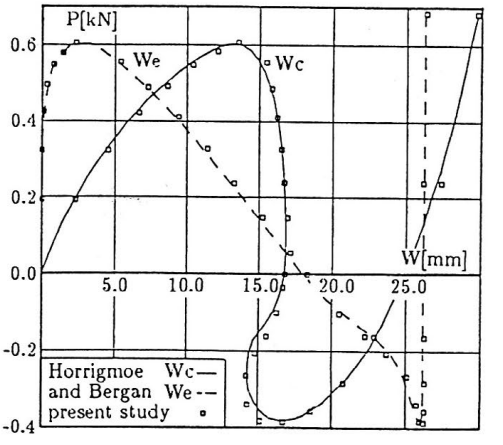

Fig. 12. Load deflection curve for a hinged cylindrical shell.

element model as shown in Fig. 9. This problem is one of the simplest test for checking the element ability to represent inextensional modes under large deflection. Comparison is provided with analytical results based on the elastica type solution where the beam is bent to a circular shape.

In Fig. 10, it is shown that good results are obtained up to rotation of about ninety degrees (= $\pi/2$). In particular, the rotation of the free end ϕ is represented to be almost linear in wide ranges.

5.6 Buckling of Cylindrical Shell

The snap-back behavior of the hinged cylindrical shell illustrates in Fig. 11 is solved by the modified Riks method[12]. A 2×2 mesh of this element is used to represent a symmetric one-quarter portion of the shell.

The local deflection which occurs at points c and e in Fig. 11 are given in Fig. 12, together with the results by Horrigmoe and Bergan[13] for comparison. The agreement is generally good and complicated snap-through behavior of the shell appears to be well represented by our analysis.

Remarks. It is noted that the required calculation time for the above problems was approximately two thirds of what had been required by a conventional selective integration element using the 3×3 Gaussian quadrature. Thus, an improved efficiency in computational costs is verified.

VI. CONCLUSION

In this paper, we propose a new stabilization procedure based on an assumed strain approach in a 9-node shell element with uniformly reduced integration. The employed stabilization procedure has clear physical backgrounds in connection with the assumed strain field, and does not need any numerical adjusting factors. It is proven by numerical examples that this element avoids a locking phenomenon without activating any spurious singular mode and it is a superior shell element excelling in a calculation efficiency.

REFERENCES

1) Parisch, H., A critical survey of the 9-node degenerated shell element with special emphasis on thin shell applications and reduced integration, Com.Meths.Appl.Mech.Eng. 20 (1979), pp.323-350.
2) Hughes, T.J.R. and Liu, W.K., Nonlinear finite element analysis of shells - part 1. Three dimensional shells, Com.Meths.Appl.Meth.Eng. 26 (1981), pp.331-362.
3) Belytschko, T., Ong, J.S.J. and Liu, W.K., A consistent control of spurious singular modes in the lagrange element for laplace and mindlin plate equations, Com.Meths.Appl.Meth.Eng. 44 (1984), pp.269-295.
4) Belytschko,T., Stolarski, H., Liu, W.K., Carpenter, N. and Ong, J.S.J., Stress projection for membrane and shear locking in shell finite element, Com.Meths.Appl.Mech.Eng. 51 (1985), pp.221-258.
5) Belytschko, T., Lin, J.I. and Tsay, C.S., Explicit algorithms for the nonlinear dynamics of Shells, Com.Meths.Appl.Meth.Eng. 42 (1984), pp.225-251.
6) Liu, W.K., Law, E.S., Lam, D. and Belytschko, T., Resultant-stress degenerated-shell element, Com.Meths.Appl.Mech.Eng. 55 (1986), pp.259-300.
7) Bathe, K.J. and Dvorkin, E.N., A formulation of general shell elements - The use of mixed interpolation of tensorial components, Com.Meths.Appl.Mech.Eng. 22 (1986), pp.697-722.
8) Huang, H.C. and Hinton, E., A new nine node degenerated shell element with enhanced membrane and shear iterpolation, Int.J.Num.Meth.Eng. 22 (1986), pp.73-92.
9) Park, K.C. and Stanley, G.M., A curved C^0 shell element based on assurmed natural-coordinate strains, J.Appl.Mech. 53 (1986), pp.278-290.
10) Hughes, T.J.R. and Winget, J. : Finite rotation effects in numerical integration of rate constitutive equations arising in large-deformation analysis, Int.J.Num.Meths.Eng. 14 (1979), pp.179-200.
11) MacNeal, R.H. and Harder, R.L., A proposed standard set of problems to test finite element, Finite Elements in Analysis and Design, 1 (1985), pp.3-20.
12) Ramm, E., The Riks/Wempner approach - An extension of the displacement control method in nonlinear analysis, Recent Advances in Nonlinear Computaional Mechanics, Hinton, E., Owen, D.J.R. and Taylor, R.L. (eds.), (Pineridge Press, 1982), pp.63-86.
13) Horrigmoe, G. and Bergan, P.G. : Nonlinear analysis of free-form shells by flat finite elements, Com.Meths.Appl.Mech.Eng. 16 (1978), pp.11-35.